How does the SST variability over the western North Atlantic Ocean control Arctic warming over the Barents-Kara Seas?

Ok Jung[1], Mi-Kyung Sung[1], Kazutoshi Sato[2], Young-Kwon Lim[3], Seong-Joong Kim[4], Eun-Hyuk Baek[4], Jee-Hoon Jeong[5], and Baek-Min Kim[4]

[1]Ewha University-Industry Collaboration Foundation, Seoul, Korea

[2]National Institute of Polar Research, Tachikawa, Japan

[3]NASA Goddard Space Flight Center / Global Modeling and Assimilation Office, Goddard Earth Sciences Technology and Research / I.M. Systems Group, Greenbelt, MD, USA

[4]Korea Polar Research Institute, Incheon, Korea

[5]Chonnam National University, Gwangju, Korea

Short Title: SST variability and Arctic warming over the Barents-Kara Seas

Corresponding author address: Dr. Baek-Min Kim, Department of Polar Climate Change Research, Korea Polar Research Institute, 26 Songdomirae-ro, Yeonsu-gu, Incheon 406-840, Korea
E-mail: bmkim@kopri.re.kr

Abstract

Arctic warming over the Barents-Kara Seas and its impacts on the mid-latitude circulations have been widely discussed. However, specific mechanism that brings the warming still remains unclear. In this study, a possible cause of the regional Arctic warming over the Barents-Kara Seas during early winter (October-December) was suggested. We found that warmer sea surface temperature anomalies over the western North Atlantic Ocean (WNAO) modulate the transient eddies overlying the oceanic frontal region. The altered transient eddy vorticity flux acts as a source for the Rossby wave straddling the western North Atlantic and the Barents-Kara Seas (Scandinavian pattern), and induces a significant warm advection, increasing surface and lower-level temperature over the Eurasian sector of the Arctic Ocean. The importance of the sea surface temperature anomalies over the WNAO and subsequent transient eddy forcing over the WNAO was also supported by both of specially designed simple model experiments and general circulation model experiments.

Keywords : Arctic warming, Stationary wave model, transient eddy vorticity forcing, Western North Atlantic Ocean

1. Introduction

The rapid increase in Arctic temperature and retreat of sea ice have been reported and widely discussed in the scientific literatures (Comiso *et al* 2008, Stroeve *et al* 2012, Vihma 2014). The increase of Arctic temperature is most pronounced during early winter (October-December) and is not spatially uniform, but exhibits several particular regional warm cores (Screen and Simmonds 2010) including the Barents-Kara Seas, East Siberian-Chukchi Seas, and northeast Canada and Greenland. Interestingly, the atmospheric warming over each location in the Arctic is known to lead to mid-latitude cooling, but with quite different spatial patterns (Mosley-Thompson *et al* 2005, Cohen *et al* 2012, Francis and Vavrus 2012, Hanna *et al* 2014, Kim *et al* 2014, Mori *et al* 2014, Kug *et al* 2015, Nakanowatari *et al* 2015, Lim *et al* 2016). Therefore, the peculiar recent phenomena called 'Warm Arctic-Cold Continents' (Overland and Wang 2010, Overland *et al* 2015) can be effectively categorized by the regional warm cores in the Arctic.

Although there are many studies on how the above-mentioned regional Arctic warming and reduced sea ice cover over those regions could induce cold winter extremes in mid-latitudes, relatively few studies have been devoted to finding the driving mechanism for those regional Arctic warming events. Recently, a linkage between oceanic thermal condition of North Atlantic Ocean

and Arctic surface temperature has been suggested (Zhang *et al* 2013, Nakanowatari *et al* 2014, Sato *et al* 2014, Luo *et al* 2016), which is supported by other findings that both surface air temperature over the Barents-Kara Seas (BKSAT) and sea surface temperature (SST) over the western North Atlantic Ocean (WNAO) have rapidly increased in recent decades (Wu *et al* 2012; Pershing *et al* 2015; Saba *et al* 2016). It is also found that the warming over the WNAO is in association with the northward shift of SST front over the Gulf Stream (Minobe *et al* 2008, Wu *et al* 2012).

Among these studies, we revisit Sato *et al* (2014) which provides a close observational link between the Barents-Kara Seas and the western North Atlantic Ocean (WNAO), over which the northern part of the Gulf Stream passes. Using linear baroclinic model experiments, Sato *et al* (2014) suggested that the changes in the local diabatic heating in association with the poleward shift of the Gulf Stream can induce a large-scale circulation pattern travelling into the Arctic inducing significant Arctic warming. However, the linear response shown in figure 5(d) of their paper was quite weak and more importantly, missed a possible contribution from the large baroclinic eddy activities over the region, which is amply noted by other studies (Sampe *et al* 2010, Frankignoul *et al* 2011, Sung *et al* 2014). As the transient eddy forcing in the North Atlantic tends to induce the large-scale teleconnection pattern, called the Scandinavian pattern

84 (SCAND), travelling over the north Atlantic and Arctic (Bueh and Nakamura
85 2007), it is important to take into account baroclinic eddy activities.

86 In this regard, Sato *et al* (2014)'s study is incomplete, although their
87 finding casts a considerable light on the divergent perspectives about 'Warm
88 Arctic-Cold Continents' by revealing that apparent links between the Barents Sea
89 ice cover and cold Eurasian winters form just a sector of a teleconnection pattern
90 that originates remotely in the North Atlantic Gulf Stream region (Simmonds and
91 Govekar 2014). Therefore, it is worthwhile evaluating whether the warming over
92 the WNAO induces a sufficient transient eddy forcing for the large-scale
93 teleconnection pattern over North Atlantic and Arctic region.

94 In this study, we aim to provide a more plausible explanation on how the
95 warm SST anomaly in the WNAO sector modulates the Eurasian teleconnections
96 and affects warming over the Arctic, and in particular, the Barents-Kara Seas in
97 early winter. Special attention will be devoted to the role of transient eddy
98 forcing, which was not studied by Sato *et al* (2014). The relative importance of
99 transient eddy forcing to the thermal forcing was assessed by a simple model
100 specially designed to treat each forcing separately. General circulation model
101 experiments were also conducted to support observational findings and simple
102 model results.
103

2. Datasets and methods

Primary observational dataset used in this study includes Hadley Centre Sea Surface Temperature (HadISST) data with 1°×1° horizontal resolution (Rayner *et al* 2003) and the reanalysis dataset obtained from the U.S. National Centers for Environmental Prediction (NCEP)/National Center for Atmospheric Research (NCAR), which has a 2.5°×2.5° horizontal resolution Kalnay *et al* 1996). Both daily and monthly mean dataset for the 1979-2013 period were utilized in this study.

In order to investigate distinguishable influences from several independent SST modes of the North Atlantic Ocean separately, Empirical Orthogonal Function (EOF) analysis was applied for early winter (October-December) mean SST anomalies over the North Atlantic Ocean domain (95°W~15°E, 20.5°N~88°N). Latitude weighting was applied by multiplying the square root of the cosine prior to the EOF analaysis. Norh's rule of thumb (North *et al* 1982) was used to test the significance of EOF modes. Regression analysis was conducted using the obtained EOF principal component (PC) time series to retrieve the associated circulation patterns.

In this study, interannual variability of surface air temperature over the Atlantic sector of the Arctic region in early winter is represented by the

123 detrended time series of area-averaged surface air temperature over the Barents-
124 Kara Seas (BKSAT). Boxed area indicated in figure 1a was used as the area
125 average.

126 The stationary wave model (here after SWM, Ting and Yu (1998)) was
127 employed to examine the dominant forcing mechanism of stationary Rossby
128 waves. This SWM is the dry dynamical core of a fully nonlinear baroclinic model.
129 The prognostic variables include vorticity, divergence, temperature and log-
130 surface pressure with R30 truncation in the horizontal and L14 vertical levels on
131 sigma coordinates. The main forcings in this model were diabatic heating,
132 convergence of transient eddy vorticity fluxes and transient eddy heat fluxes. The
133 forcing terms can be tested using idealized distribution or diagnosed forcing
134 fields derived from observations. In this study, the latter approach was used (see
135 Supplementary Information). The three forcing terms can be defined as:

136 $$\mathrm{TF_{vor}} = -\nabla \cdot (\overline{\mathrm{V}'\xi'}) \quad (1)$$

137 $$\mathrm{TF_{temp}} = -\left(\frac{\mathrm{P}}{\mathrm{P_0}}\right)^{\mathrm{R}/\mathrm{C_p}} \left[\nabla \cdot (\overline{\mathrm{V}'\theta'}) + \frac{\partial(\overline{\omega'\theta'})}{\partial \mathrm{p}}\right] \quad (2)$$

138 $$\mathrm{Q_1} = \frac{\partial \overline{\mathrm{T}}}{\partial \mathrm{t}} + \overline{\mathrm{V}} \cdot \nabla \overline{\mathrm{T}} + \overline{\omega}\left(\frac{\partial \overline{\mathrm{T}}}{\partial \mathrm{p}} - \frac{\mathrm{R}\overline{\mathrm{T}}}{\mathrm{C_p p}}\right) - \mathrm{TF_{temp}} \quad (3)$$

139 where ξ is the vorticity, V is the horizontal wind, p is pressure, ω is the
140 pressure vertical velocity, and $\mathrm{TF_{vor}}$ and $\mathrm{TF_{temp}}$ indicate the non-linear

transient eddy vorticity flux convergence and transient eddy heat flux convergence, respectively. Q_1 indicates the monthly mean diabatic heating. Note that Q_1 used in this study is different from that in Sato *et al* (2014) because of the existence of TF_{temp} in (3). The bar represents the monthly mean and prime shows the deviation from the monthly mean. Further details of the model equations or information can be found in Ting and Yu (1998) and Wang and Ting (1999).

To investigate the impact of SST warming over the WNAO in a more realistic modelling framework, we used a fully coupled general circulation model (GCM), Climate Model Version 2.1 (CM2.1) developed by the Geophysical Fluid Dynamical Loboratory (GFDL) (Delworth *et al* 2006). As a control run, we conducted climatological equilibrium simulations with 400 ppm CO2 for 100 years. In a forced simulation, SST over the WNAO region (the box in figure 5a, i.e., 38^{o}N-48^{o}N, 55^{o}W-75^{o}W) was restored toward the prescribed warm SST conditions with 5 days restoring time scale. Accoring to Pershing *et al* (2016), the WNAO region is the highest warming place on the earth and, in the last decade, there was 2 ^{o}C increase of SST. Accordingly, we prepared the warm SST condition over the WNAO region by adding the observed SST trend of the recent 11 years (2004-2014) to the climatological SST fields of control run. Note that the model freely evolves except for the boxed region in figure 5a in the forced run. To

estimate the response to the SST forcing over the WNAO, we will analyze differences between the results of the forced run and the control run.

3. Results

3.1 Warming over Barents-Kara Seas and SCAND teleconnection pattern

As suggested by Sato *et al* (2014), during early winter, changes in surface air temperature, especially over the Barents-Kara Seas in the Atlantic sector of the Arctic Ocean, were closely related to changes in SST variability over the WNAO (figure 1(a)). In addition to the warming of WNAO, colder regional SST anomaly over the Labrador Sea was observed in association with the warmer BKSAT constituting the warm-cold-warm tri-polar pattern over a large area of the North Atlantic and European sector of the Arctic Ocean.

The warming over the Barents-Kara Seas in early winter accompanies a well-defined upper-level circulation pattern (figure 1(b)). This upper level circulation pattern resembles the EU1 or the SCAND pattern (Barnston and Livezey 1987). In fact, among the teleconnection indices archived at the National Oceanic and Atmospheric Administration (NOAA)/National Center for Environmental Prediction (NCEP)/Climate Prediction Center (CPC), the SCAND index shows the highest correlation with BKSAT. The correlation coefficient between the time series of BKSAT and the early winter mean SCAND index is 0.4,

181 with greater than 95% confidence (figure 1(c)).

182 Interestingly, the wave activity flux vectors (Plumb 1986) in figure 1(b)
183 indicate that the wave source region is over the WNAO, not over the Barents-
184 Kara Seas where sea ice loss is pronounced. A large-scale wave pattern with
185 anticyclonic centre over the WNAO emanates and exhibits a travelling Rossby
186 wave pattern toward eastern Europe, the Barents-Kara Seas, and eventually
187 reaching the northeast Asia. In particular, a strong positive upper level
188 geopotential height anomaly over the western North Atlantic region matches the
189 positive SST anomaly over the WNAO. Therefore, the warm SST in figure 1(a)
190 over western North Atlantic region seems to play an important role in the
191 teleconnection. Furthermore, the cold SST anomaly over the Labrador Sea and
192 warm SST anomalies over the Barents-Kara Seas in figure 1(a) also match well
193 with the geopotential height anomalies in figure 1(b).

194 Combining the results displayed in figure 1, we set a series of working
195 hypotheses that can be tested by simple numerical modelling experiments: 1)
196 Interannual variability of the BKSAT is, in fact, largely originated from the
197 WNAO. 2) Warmer SST anomaly over the WNAO causes warm temperature
198 anomalies over the Barents-Kara Seas via upper-level planetary wave
199 propagation, similar to SCAND and associated warm advection.

200

3.2 EOF analysis on North Atlantic SST variabilities

Prior to verifying the above hypotheses, we conducted EOF analysis to determine whether there exists an identifiable North Atlantic SST variability linked to the Arctic warming over the Barents-Kara Seas. The early winter averaged SST anomalies during the 1979–2013 period were decomposed into three dominant modes: the first mode (EOF1) explains 36.6% of the total variance and exhibits a strong linear trend. The spatial pattern of EOF1 shows apparent warming over the entire North Atlantic basin. Although the pattern contains significant SST warming over the Barents-Kara Seas, the correlation between the PC1 and BKSAT is low (0.07). Note that BKSAT is a detrended index.

The second mode explains 14.5% of the variance, and has three centres of action which are located over the western North Atlantic Ocean, the northern North Atlantic Ocean, and the eastern North Atlantic (figure 2(c)). The temporal correlation coefficient between the second PC and BKSAT time series is very low (0.03) indicating no significant relationship, as with EOF2 showing no anomalies in the Arctic Sea region. The most similar pattern to the regressed pattern depicted in figure 1(a) is described in EOF3, which shows a tri-polar pattern with warm SST anomaly over the WNAO; cold over the south of Greenland and Labrador Seas, and warm over the Barents-Kara Seas. The similarity is quite remarkable. As expected by the warm centre over the Barents-Kara Seas in figure

2(e), the PC3 time series shows a significant correlation with the BKSAT time series (corr.=0.4) at 99% confidence level (figure 2(f)). The PC3 time-series also has a high correlation coefficient with the SCAND index (corr.=0.57) (table 1). According to the North's rule of thumb, the three EOF modes are well separated (North *et al* 1982).

It is notable that the SST anomaly over the WNAO lies over the northern edge of the Gulf Stream, which shows strong SST gradient (see isotherms in figure 2(e)). The warm SST anomaly over this region may represent the poleward shift of the Gulf Stream and intense baroclinic zone. Since it is well-known that the SST gradient associated with the western boundary current is known to be a great source of baroclinicity (Minobe *et al* 2008), it is the source of available potential energy for the growth of transient eddies. This leads us to investigate the role of transient eddies in the large-scale teleconnection pattern that links the North Atlantic and the Arctic regions.

3.3 Physical mechanism of Atlantic origin of Arctic warming

Atmospheric circulation features related with the EOF3 of SST variability are depicted in figure 3. Geopotential height anomaly at 250hPa representing the upper-level circulation features a wave train pattern emanating from the WNAO toward Eurasia across the north-eastern Atlantic and the Barents-Kara Seas

241 (contour in figure 3(a)). As expected by the similarity between the SST anomaly
242 regressed onto the BKSAT (figure 1(a)) and the EOF third mode (figure 2(e)), this
243 upper-level circulation pattern is similar to the SCAND pattern in figure 1(b).
244 The response is equivalent barotropic (contour in figure 3(a) and 3(b)) and,
245 therefore, the regressed surface air temperature anomaly (shaded in figure 3(a))
246 is in gereral in phase with the upper-level geopotential height anomaly. The
247 significant warming over Barents-Kara Seas can partly be explained by the
248 enhanced warm advection along the western edge of the anticyclonic anomaly
249 over western Europe induced by this barotropic large-scale anomaly at lower-
250 levels (figure 3(b)).

251 In association with the downstream propagation of SCAND toward east
252 Asia, cold temperature anomalies appear primarily over Central and East Asia,
253 where upper-level cyclonic response dominates (figure 1(b)). In this case, the
254 upper-level cyclonic response reduces the thickness of the air column over East
255 Asia and therefore, the column average temperature drops. Combined with the
256 climatologically strong northerly flow in this region, strong cold advection is
257 induced. The warm and cold anomalies explained above resembles 'Warm
258 Arctic-Cold Continents' or 'Warm Arctic-Cold Siberia' pattern (Overland *et al*
259 2011, Inoue *et al* 2012, Kim *et al* 2014, Mori *et al* 2014, Kug *et al* 2015).

260 Returning to the North Atlantic, the source region of the wave train seems

261 to lie at the WNAO region (box in figure 2(e)). Compared with the EOF3 in figure
262 2(e), this wave activity source region coincides with the warm SST anomaly over
263 the WNAO. Sato *et al* (2014) examined the possible role of the diabatic heating
264 over the WNAO by calculating the apparent heat source and resultant linear
265 stationary eddy response. In this work, we investigated another possibility. The
266 warm SST anomaly over the WNAO can be interpreted as the northward
267 extension of the Gulf stream (Wu *et al* 2012) indicating northward shift of the
268 ocean front. Since the WNAO region exhibits strong SST gradients as shown in
269 figure 2(e), we expect that the warm SST anomaly could alter the activities of
270 synoptic-scale eddies which are sensitive to the temperature gradient and
271 diabatic heat sources (Brayshaw *et al* 2008, Nakamura *et al* 2008). Indeed, the
272 transient eddy activities estimated by the variance of the 300-hPa daily
273 meridional wind anomaly regressed to EOF3 also shifted eastward compared
274 with its climatological position (figure 3(c)) and the northward shift of Atlantic
275 sub-polar jet occured at the same time (figure 3(d)). These results are consistent
276 with the previous studies that addressed the importance of the SST gradient in
277 the alteration of transient eddy activities (Sampe *et al* 2010, Frankignoul *et al* 2011,
278 Sung *et al* 2014).

279 Combined changes in the transient eddy activities and Atlantic sub-polar
280 jet in association with the SST variability over the WNAO hint the possible role of

transient eddy activities on large-scale teleconnection patterns (Bueh and Nakamura 2007, Lim and Kim 2016). To investigate the relative role of transient eddies linked to SST variability over the WNAO, we used the SWM alternatively forced by diabatic heating or transient eddy forcing and estimated the relative importance of each forcing term by comparing the SWM responses forced by each forcing term separately (see Supplementary Information).

Forcings and associated responses of SWM experiments are represented in figure 4. Within the boxed region of the WNAO, the negative TF_{vor} in figure 4(a) was consistent with significant high anomalies shown in figure 1(b). Interstingly, the diabatic forcing in figure 4(c) and convergence of transient eddy heat flux compensated each other, meaning that the diabatic heating was largely balanced by eddy heat transport.

As noted previously, the WNAO region is a key region of strong SST variability and is associated with the large changes in SST gradient and in storm track. We examined the relative importance of these three forcings in the excitation of large-scale circulation. As shown in figure 4, a major response was obtained with transient eddy vorticity forcing and this forcing reproduced the SCAND wave structure remarkably (compare figure 3(a) and figure 4(a)). In addition, the wave-like feature in the model response had a high correlation with observed SCAND pattern (0.62). Relatively weaker contribution was obtained

from the transient eddy temperature forcing and total diabatic heating forcing. Considering that we only applied the forcing in the restricted region (black box in figure 4), the result is rather surprising and confirms that the important role of the storm activities in large-scale teleconnection patterns. These results provide evidence that transient vorticity flux related to the SST interannual variability over the WNAO is a key factor for the SCAND teleconnection pattern.

The last evidence of the importance of SST over the WNAO for the Arctic warming comes from fully coupled model experiments (figure 5). In general, model successfully captures various features depicted in the observational analysis results: Model SST response in figure 5(a) shows the warm-cold-warm SST pattern similar to the EOF3 pattern (figure 2(e)). Considering that the SST nudging was only applied to the boxed region in figure 5(a) in the model simulation. Therefore, the warm SST anomaly over the Barents-Kara Seas was internally generated by the fully coupled model as a response. The upper-level response was also reproduced reasonably well (figure 5(b)). Therefore, the results from the regression analysis (figure 1 and 3) are supported by the fully coupled model experiments.

4. Summary and Discussion

Sato *et al* (2014) showed that the poleward shift of the Gulf Stream

influences the increase (decrease) of temperature (sea ice extent) over the Barents-Kara Seas and cooling over Eurasia through planetary waves triggered over the Gulf Stream region. In this study, the origin of the planetary waves are investigated in detail.

First, we show that the variability in the surface air temperature over the Barents-Kara Seas is largely controlled by two dominant SST modes in the domain including the North Atlantic Ocean and the Atlantic sector of Arctic Ocean. The warming trends in both the Atlantic Ocean and the Barents-Kara Seas are largely depicted by EOF first mode and this pattern resembles the basin-wide warming pattern. On the other hand, interannual variability is controlled by the tri-polar SST pattern depicted as EOF third mode in this study. The third SST mode represents the poleward shift of the Gulf Stream and accompanying changes in storm track as indicated by Sato *et al* (2014).

Through a simple modelling study using SWM, we concluded that the altered upper-level transient eddy vorticity forcing in association with the changes in the storm track plays a major role in the generation of the SCAND pattern and therefore, plays a bridging role between the North Atlantic Ocean and the Atlantic sector of Arctic in early winter at the interannual time-scale. We could reproduce an upper-level circulation pattern that was very similar to SCAND only with altered transient eddy vorticity forcing in the upper-level.

341 The surface warm advection along the high pressure center of SCAND at
342 the Barents-Kara Seas, which is essentially barotropic is an important source of
343 warming of BKSAT. The direct influence of the diabatic heating over the WNAO
344 sector was relatively minor compared to the transient forcing.

345 Although this study emphasizes the importance of the enhanced transient
346 eddy forcing during the warm period of the WNAO, it should be noted that a
347 large portion of the warming is also contributed by the subsequent reduction of
348 sea ice concentration over the Barents-Kara Seas through the enhanced energy
349 fluxes from the Arctic Ocean (figure A1 in supplementary information). However,
350 in this study, we did not conduct any quantitative assessments on that part since
351 we are only interested in the Atlantic origin of the warming.

352 It is still unknown why the transient eddy activities show those systematic
353 behaviors responding to the specific SST patterns over the North Atlantic Ocean.
354 To deal with this issue, we need to understand how individual Atlantic storms
355 respond to warm SST over the WNAO by tracking storm intensity and its
356 passage (storm track) along the storm. Both systematic changes in storm intensity
357 and track in association with the particular SST pattern over the North Atlantic
358 should collectively contribute to the monthly-timescale transient eddy forcing.
359 We are currently investigating this problem by tracking individual Atlantic
360 storms.

Acknowledgements

We thank the two reviewers for their helpful comments. This work is conducted to fulfill the task assigned to the project of Korea Polar Research Institute titled "Development and Application of the Korea Polar Prediction System (KPOPS) for Climate Change and Disasterous Weather Events". First author, Jung Ok, is partly supported by "Development of cloud-precipitation Algorithms" project, funded by ETRI, which is a subproject of "Development of Geostationary Meteorological Satellite Ground Segment (NMSC-2016-01)" program funded by NMSC (National Meteorological Satellite Center) of KMA(Korea Meteorological Administration). Jee-Hoon Jeong is supported by the Korea Meteorological Administration Research and Development Program (KMIPA2015-2091).

References

Barnston A.G., and Livezey R.E. (1987), Classification, Seasonality and Persistence of Low-Frequency Atmospheric Circulation Patterns, *Mon. Weather Re., 115,* 1083–1126.

Brayshaw D.J., Hoskins B. and Blackburn M. (2008), The storm-track response to idealized SST perturbations in an Aquaplanet GCM, *J. Atmos. Sci., 65,* 2842-2860.

Bueh C., and Nakamura H. (2007), Scandinavian pattern and its climatic impact, *Q. J. R. Meteorol. Soc., 133,* 2117–2131.

Cohen J.L., Furtado J.C., Barlow, M.A., Alexeev, V.A. and Cherry J.E. (2012), Arctic warming, increasing snow cover and widespread boreal winter cooling, *Environ. Res. Lett., 7*, 1-8.

Comiso J.C., Parkinson C.L., Gersten R. and Stock L. (2008), Accelerated decline in the Arctic sea ice cover, *Geophys. Res. Lett., 35,* 1–6.

Delworth, T. L. et al. (2006), GFDL's CM2 global coupled climate models. Part I: Formulation and simulation characteristics, *J. Clim.*, *19*(5), 643–674, doi:10.1175/JCLI3629.1.

Francis, J.A. and Vavrus S.J. (2012) Evidence linking Arctic amplification to extreme weather in mid-latutudes, *Geophys. Res. Lett. 39,* 1-6.

Frankignoul, C., Sennéchael N., Kwon Y.-O., and Alexander M. A. (2011), Influence of the Meridional Shifts of the Kuroshio and the Oyashio Extensions on the Atmospheric Circulation, *J. Clim., 24(3),* 762-777.

Hanna E., Fettweis X., Mernild S.H., Cappelen J., Ribergaard M.H., Shuman C.A., Steffen K., Wood L., and Mote T.L. (2014), Atmospheric and oceanic climate forcing of the exceptional Greenland ice sheet surface melt in summer 2012, *Int. J. Climatol., 34,* 1022–1037.

Inoue J, Hori M.E., and Takaya K. (2012), The role of Barents Sea ice in the wintertime cyclone track and emergence of a warm-arctic cold-Siberian anomaly, *J. Clim., 25,* 2561–2568.

Kalnay E. et al., (1996), The NCEP/NCAR 40-year reanalysis project, *Bull. Am. Meteorol. Soc., 77,* 437–471.

Kim B.-M., Son S.-W., Min S.-K., Jeong J.-H., Kim S.-J., Zhang X., Shim T.-H., and Yoon J-H (2014), Weakening of the stratospheric polar vortex by Arctic sea-ice loss, *Nat. Commun., 5,* 4646.

Kug, J.-S., Jeong J.-H., Jang Y.-S., Kim B.-M., Folland C.K., Min S.-K., and Son S.-W. (2015), Two distinct influences of Arctic warming on cold winters over North America and East Asia, *Nature Geoscience*, *8*, 759-762.

Lim Y.K., and Kim H.D. (2016), Comparison of the impact of the Arctic Oscillation and Eurasian teleconnection on interannual variation in East Asian winter temperatures and monsoon, *Theor. Appl. Climatol., 124,* 267-279.

Lim Y.-K., Schubert S.D., Nowicki S.M., Lee J.N., Molod A.M., Cullather R.I, Zhao B.,and Velicogna I., (2016), Atmospheric summer teleconnections and Greenland ice sheet surface mass variations: Insights from MERRA-2., *Environ. Res. Lett., 11,* 024002.

Luo D., Xiao Y., Yao Y., Dai A., Simmonds I., and Franzke C. L. E. (2016), Impact of Ural blocking on winter warm arctic-cold Eurasian anomalies. Part I: blocking-induced amplification, *J. Clim., 29,* 3925-3947.

Minobe S., Yoshida-Kuwano A., Komori N., Xie S. P., and Small R. J. (2008), Influence of the Gulf Stream on the troposphere, *Nature, 452,* 206–209.

Mori M., Watanabe M., Shiogama H., Inoue J. and Kimoto M. (2014), Robust Arctic sea-ice influence on the frequent Eurasian cold winters in past decades, *Nat. Geosci., 7,* 869–873.

Mosley-Thompson E., Readinger C.R., Craigmile P., Thompson L.G., Calder C.A. (2005), Regional sensitivity of Greenland precipitation to NAO variability, *Geophys. Res. Lett., 32,* L24707.

Nakanowatari T., Sato K., and Inoue J. (2014), Predictability of the Barents Sea ice in early winter:

remote effects of oceanic and atmospheric thermal conditions from the North Atlantic, *J. Clim., 27,* 8884–8901

Nakanowatari, T., Inoue J., Sato K., and Kikuchi T. (2015), Summertime atmosphere-ocean preconditionings for the Bering Sea ice retreat and the following severe winters in North America, *Environ. Res. Lett., 10*(9).

Nakamura H., Sampe T., Goto A., Ohfuchi W., and Xie S.P. (2008), On the importance of midlatitude oceanic frontal zones for the mean state and dominant variability in the tropospheric circulation, *Geophys. Res. Lett., 35,* L15709.

North G.R., Bell T.L., Cahalan R.F., and Moenig F.J. (1982), Sampling errors in the estimation of empirical orthogonal functions, *Mon.Weather Rev., 110,* 669–706.

Overland, J.E., and Wang M. (2010), Large scale atmospheric circulation changes are associated with the recent loss of Arctic sea ice, *Tellus A, 62*(1), 1-9.

Overland J. E., Wood K. R., and Wang M. (2011), Warm Arctic-cold continents: climate impacts of the newly open Arctic sea, *Polar Res., 30,* 15787.

Overland J. E., Francis J. A., Hall R., Hanna E., Kim S.-J., and Vihma T. (2015), The melting Arctic and mid-latitude weather patterns: are they connected?, *J. of Clim., 28,* 7917-7932.

Pershing A.J., et al. (2015), Slow adaptation in the face of rapid warming leads to collapse of the Gulf of Maine cod fishery, *Science, 350,* 809–812.

Plumb R.A. (1986), Three-Dimensional Propagation of Transient Quasi-Geostrophic Eddies and Its Relationship with the Eddy Forcing of the Time—Mean Flow, *J. Atmos. Sci., 43,* 1657–1678.

Rayner N.A., Parker D.E., Horton E.B., Folland C.K., Alexander L.V., Rowell D.P., Kent E.C., and Kaplan A. (2003), Global analyses of sea surface temperature, sea ice, and night marine air temperature since the late nineteenth century, *J. Geophys. Res. Atmos., 108,* 002670.

Saba V.S., et al. (2016), Enhanced warming of the Northwest Atlantic Ocean under climate change, *J. of Geophys. Res. Oceans, 121,* 118–132.

Sampe T., Nakamura H., Goto A., and Ohfuchi W. (2010), Significance of a Midlatitude SST Frontal Zone in the Formation of a Storm Track and an Eddy-Driven Westerly Jet*, *J. Clim., 23(7),* 1793-1814.

Sato K., Inoue J., and Watanabe M. (2014), Influence of the Gulf Stream on the Barents Sea ice retreat and Eurasian coldness during early winter, *Environ. Res. Lett., 9,* 084009.

Screen J.A., and Simmonds I. (2010), Increasing fall-winter energy loss from the Arctic Ocean and its role in Arctic temperature amplification, *Geophys. Res. Lett., 37,* L16707, doi:10.1029/2010g1044136.

Simmonds I., and Govekar P.D. (2014), What are the physical links between Arctic sea ice loss and Eurasian winter climate? *Environ. Res. Lett., 9,* 101003.

Stroeve J.C., Kattsov V., Barrett A., Serreze M., Pavlova T., Holland M., and Meier W. N. (2012), Trends in Arctic sea ice extent from CMIP5, CMIP3 and observations, *Geophys. Res. Lett., 39,* L16502.

Sung, M.-K., An S.-I., Kim B.-M., and Woo S.-H. (2014), A physical mechanism of the precipitation dipole in the western United States based on PDO-storm track relationship, *Geophys. Res. Lett., 41*(13), 4719-4726.

Ting M., and Yu L. (1998), Steady response to tropical heating in wavy linear and nonlinear baroclinic models, *J. Atmos. Sci., 55,* 3565–3582.

Vihma T. (2014), Effects of Arctic sea ice decline on weather and climate: a review, *Surv. Geophys., 35,* 1175–1214.

Wang H., and Ting M. (1999), Seasonal cycle of the climatological stationary waves in the NCEP-NCAR Reanalysis, *J. Atmos. Sci., 56,* 3892–3919.

Wu L. et al. (2012), Enhanced warming over the global subtropical western boundary currents, *Nature Clim. Change*, 2, 161–166.

Zhang X., He J., Zhang J., Polyakov I., Gerdes R., Inoue J., and Wu P. (2013), Enhanced poleward moisture transport and amplified northern high-latitude wetting trend, *Nature Clim. Change*, *3*, 47–51.

Tables and Figures

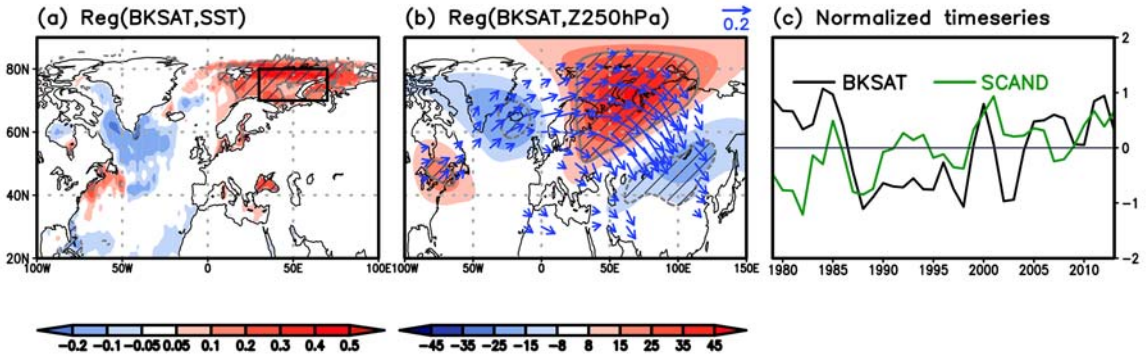

Figure 1. Regression of early winter mean (OND mean) (a) SST and (b) 250 hPa geopotential height and wave activity on the detrended surface air temperature anomalies over Barents-Kara Sea region (BKSAT, 30°~70°E, 70°~80°N), denoted by the black box in Figure 1(a). (c) Normalized time series of Scandinavian teleconnection index (SCAND, green line) and detrended BKSAT (black line). Hatch represents significance at 95% level of confidence.

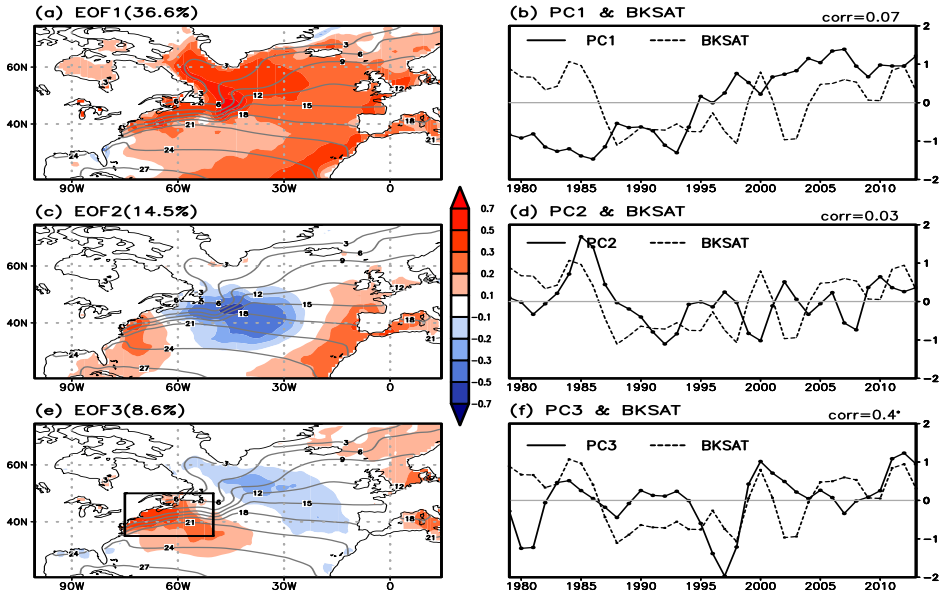

Figure 2. EOF analysis applied to SST anomalies over the North Atlantic Ocean. (a) First EOF mode (EOF1) of the early winter mean (OND mean) SST anomaly (shading) and its climatology (contour). (c) and (e) are same as (a) except for the second and third EOF modes. (b) the corresponding PC1 time series for EOF1 (solid line). (d) and (f) are same as (a) except for the PC time series corresponding to the second and third EOFs. Dashed line in (b), (d) and (f) denotes the time series of detrended BKSAT. Temporal correlation between eah PC time series and BKSAT is provided in each panel at the upper-right corner. Box region (75°~50°W, 35°~50°N) indicates the WNAO region.

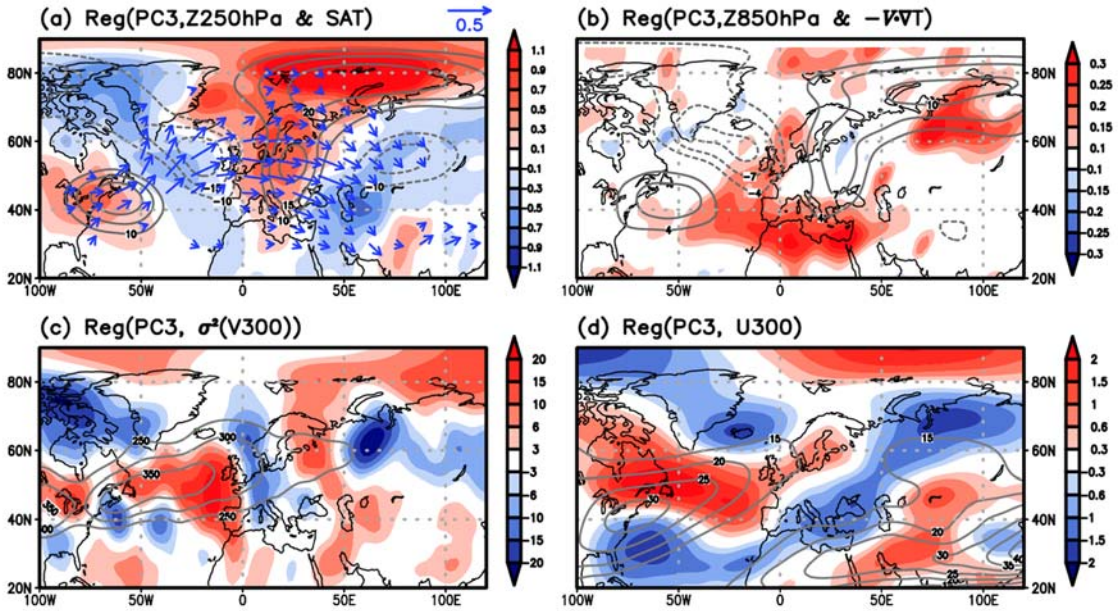

Figure 3. Regression maps constructed using PC3 time series for (a) surface air temperature (shading), geopotential height at 250hPa (contour) and wave activity flux (vector), (b) low-level temperature advection anomaly (1000hPa-850hPa) (shading) and geopotential height at 850hPa (contour), (c) variance of meridional wind at 300hPa (shading) and its climatology (contour) and (d) zonal wind at 300hPa (shading) and its climatology (contour).

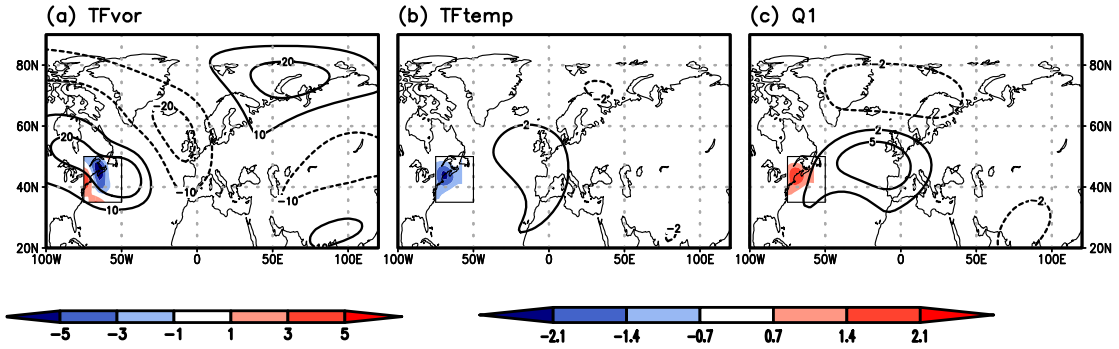

Figure 4. Model response of geopotential height at 300 hPa forced by (a) transient eddy vorticity forcing, (b) transient temperature forcing and (c) diabatic heat source. Forcing is only applied to the boxed region (75°~50°W, 35°~50°N). In (a), transient eddy vorticity forcing at 300 hPa is represented. Values are normalized by 10^{11}. In (b) and (c), vertically integrated forcing terms from 925 hPa to 300 hPa are represented and again normalized by 10^{6}. Model streamfunction response is converted to geopotential height by multiplying 10^{-5} divided by gravity.

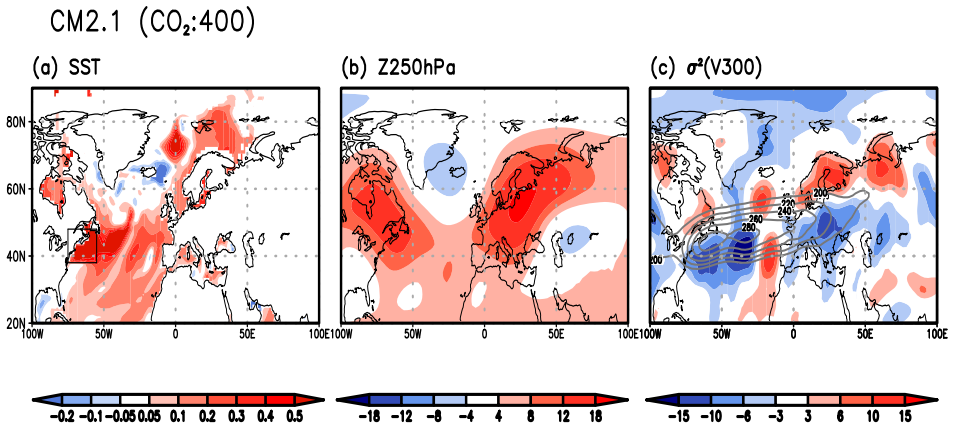

(b) 250hPa response is ın. In forced

518 Table 1. Correlation coefficients among the atmospheric teleconnection modes and the
519 PC time series.

	SCAND	EAWR	NAO
PC1	0.1	0.29	0.37
PC2	0.1	0.48*	0.02
PC3	0.57*	0.10	0.4

520 *Statistically significant at $p < 0.01$.

Supplementary Information

Regression analysis result for sea ice concentration:

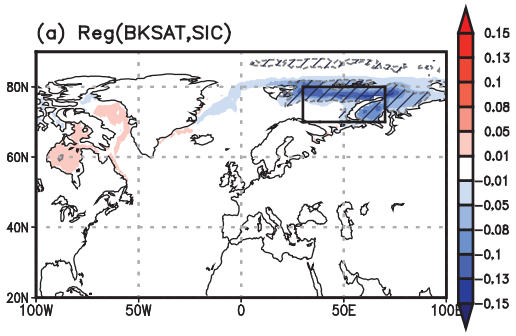

Figure A1. Regressed early winter mean (OND mean) sea ice concentration (SIC) onto the detrended surface air temperature anomalies over Barents-Kara Seas region (BKSAT, 30°~70°E, 70°~80°N), denoted by the black box in Figure 1(a).

Preparation of TF_{vor} in eq. (1), TF_{temp} in eq. (2), and Q_1 in eq. (3) using reanalysis data:

In this study, we prepared the forcing terms in eq. (1)-(3) for SWM using observational data. This method is different from the previous studies which used the idealized forcing [i.e., *Schubert et al.,* 2011; *Lim* 2015]. To diagnose the forcing terms, we first calculated the transient eddy vorticity forcing, TF_{vor} in eq. (1), and transient temperature forcing, TF_{temp} in eq. (2) using daily fields of reanalysis data. As noted in methods section, TF_{vor} and TF_{temp} indicate the non-linear transient eddy vorticity flux convergence and transient eddy heat flux convergence, respectively. Q_1 in (3) is calculated using TF_{temp} suggested by Wang and Ting [1999]. The bar represents the monthly mean and prime represents the deviation from the monthly mean. Next, the three forcing terms were regressed onto PC3 time series (Figure 2(f)). To focus on the

role of the SST variability over the WNAO region, forcing terms were restricted to the geographically confined region of 75°~50°W, 35°~50°N where SST showed the large warming anomaly. We also calculated the divergence of vertically averaged transient eddy heat flux (TF_{temp}) from 925 hPa to 300 hPa regressed onto the PC3 time series (Figure 4(b)).

References

Lim Y.-K. (2015), The East Atlantic West Russia teleconnection in the North Atlantic: Climate impact and relation to Rossby wave propagation, *Clim. Dyn.*, *44*, 3211–3222.

Schubert S., Wang H., and Suarez M. (2011), Warm season subseasonal variability and climate extremes in the Northern Hemisphere: the role of stationary Rossby waves, *J. Clim.*, *24*, 4773–4792.